OPTIMIZATION OF LOWER HYBRID WAVE COUPLING FOR THE WEST LHCD LAUNCHERS

A.S. LIANG
Southwestern Institute of Physics
Chengdu, China
Email: liangas@swip.ac.cn

A.S. LIANG, A. EKEDAHL, L. DELPECH, M. GONICHE, J. HILLAIRET, J. MORALES, R. NOUAILLETAS, X. REGAL-MEZIN and the WEST Team*
CEA, IRFM
Saint Paul-lez-Durance, France

Abstract

The lower hybrid current drive (LHCD) system in WEST plays a key role in achieving long pulse operation and high-performance plasmas. Up to 5.3 MW LHCD power has been coupled in WEST plasmas and a pulse duration of 55 s has been sustained with 3 MW of LHCD. The LHCD power is launched into the plasma by two multijunction launchers (Full-Active-Multijunction and Passive-Active-Multijunction), previously used in Tore Supra. Before the start of WEST, the front face of the Full-Active-Multijuntion (FAM/LH1) launcher was reshaped in the toroidal direction to fit the toroidal curvature of the WEST plasmas, since the toroidal ripple in WEST is smaller than that in the former Tore Supra. The paper presents an analysis of the LH wave coupling on the two LHCD launchers, in different plasma configurations and at different edge electron densities.

1. INTRODUCTION

WEST provides an integrated platform for testing ITER-like divertor components in a tokamak environment under combined heat and particle loads [1]. It will allow assessing the power handling capability and lifetime of ITER high heat flux tungsten divertor components under ITER-relevant power loads (10-20 MW/m^2), particle fluence (~ 10^{27} D/m^2) and time scales. The additional plasma heating and current drive in WEST is provided by radiofrequency methods only, i.e. ion cyclotron resonance heating (ICRH) [2] and lower hybrid current drive (LHCD). The 3.7 GHz LHCD system is composed of two multijunction launchers, named Full-Active-Multijunction (FAM/LH1) and Passive-Active-Multijunction (PAM/LH2), fed by 16 klystrons TH2103C with a capacity of ~ 600 kW each in CW conditions. The CFC side protections used in Tore Supra are reused for WEST, with an added W-coating on a layer of molybdenum (80 µm Mo + 80 µm W). The launchers with side protections are moveable radially between shots.

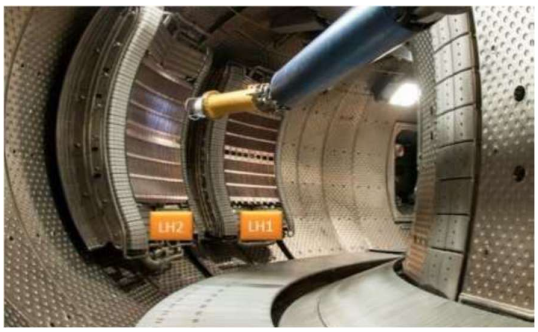

FIG. 1. Photograph of the two LHCD launchers inside the WEST vacuum vessel. The Articulated Inspection Arm is also visible on the photo.

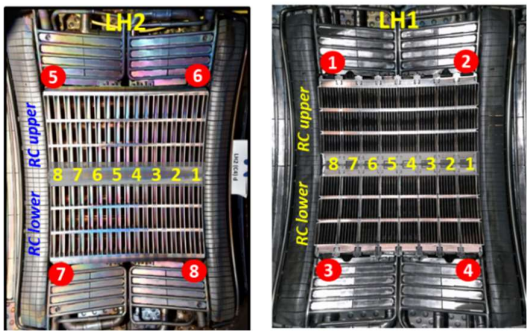

FIG. 2. Photos of the LH2 launcher (left) and the LH1 launcher (right). The numbering of the waveguide modules and the Langmuir probes are indicated.

Before the start of WEST, the front face of the FAM/LH1 launcher was reshaped in the toroidal direction to fit the toroidal curvature of the WEST plasmas [3], since the toroidal ripple in WEST is smaller than that in the former Tore Supra. In contrast, the PAM/LH2 launcher can to a larger extent tolerate the toroidal mismatch, owing to its better coupling close to the cut-off density [4]. The PAM/LH2 launcher has therefore not yet been reshaped for the experiments carried out in WEST Phase I.

*http://west.cea.fr/WESTteam

2. MAIN LHCD RESULTS IN WEST PHASE I

In the 2019 and 2020-21 campaigns, the LHCD coupled power has reached up to 5.3 MW in L-mode plasmas. In combination with ICRH, the maximum additional heating power reached so far is 8.8 MW [5]. Experiments have been performed in X-point plasmas in both Lower Single Null (LSN) and Upper Single Null (USN) configurations, with plasma current, I_P, between 0.3 MA and 0.7 MA (q_{95} between 3 and 6), central line integrated electron density (n_{li}) between 2.5 and 8.5×10^{19} m^{-2} (n_e/n_{GW} = 0.3-0.8). Fig. 3 shows the time traces of the maximum LHCD power reached in WEST. Good coupling was achieved on both launchers, with an average power reflection coefficient of ~3% on both LH1 and LH2. This pulse was carried out in the LSN configuration (Fig. 4) with the last closed flux surface at the mid-plane, R_{ext}, of 2.97 m. According to the NICE equilibrium reconstruction [6], the plasma centre was shifted above the mid-plane, resulting in a poloidally asymmetric plasma shape in front of the LH launchers, as seen in Fig. 4. Good coupling was nevertheless obtained on both the upper and lower rows of the LH launchers (Fig. 3b and Fig. 3c). During experiments, the Equatorial Radial Outer Gap (EROG) is feedback controlled via the plasma control system (PCS) [7], while the UROG (Upper ROG) and LROG (Lower ROG) are controlled in feedforward by tuning the currents in the low field side coils from shot to shot.

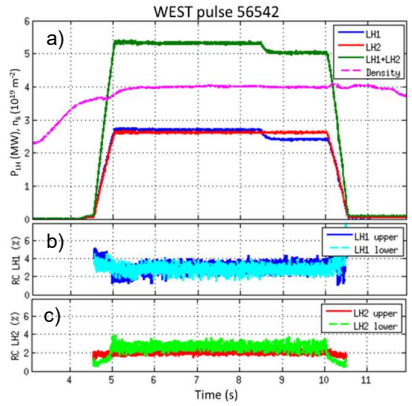

FIG. 3. L-mode discharge with 5.3 MW coupled LHCD power (a). Average power reflection coefficient (RC) on the upper and lower rows of LH1 (b) and LH2 (c).

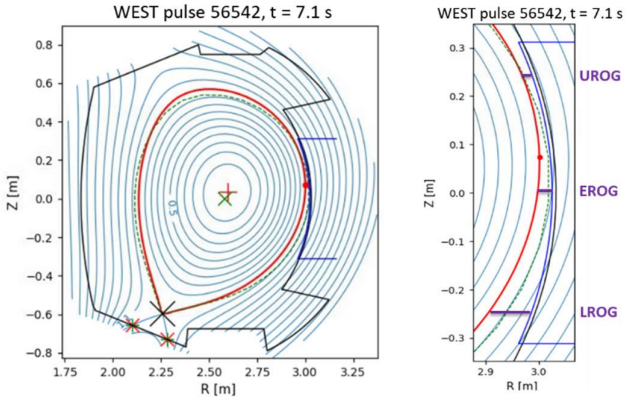

FIG. 4. Plasma equilibrium for pulse #56542. The red line indicates the last closed flux surface from the NICE-code [6]. The upper, lower and equatorial radial outer gaps are indicated.

3. EFFECT OF TOROIDAL RESHAPING ON LH1

The first LHCD experiments in WEST were carried out in LSN configuration with the radius of the last closed flux surface at the mid-plane, R_{ext}, around 2.98 m. The LH launchers were positioned at ~ 3.01 m, i.e. approximately 3 cm from the last closed flux surface. Fig. 5 shows the power reflection coefficient (RC) in each module on the upper half of FAM/LH1 versus the density measured by a Langmuir probe on the upper part of the LH1 launcher (indicated in Fig. 2), for a database of around 40 pulses with a plasma current of 500 kA (pulse number range #53813-54106). The ALOHA modelling [8] for the upper part of LH1 using two density gradients (λ_1 = 1 mm; λ_2 = 15 mm) is also plotted. Fig. 5 illustrates that RC in all modules behave similarly and decrease when the density on the probe increases. This indicates that the density is homogeneous along the toroidal direction and thus that the reshaping of the launcher mouth has been efficient. Besides, a quite good agreement with the ALOHA calculation is found.

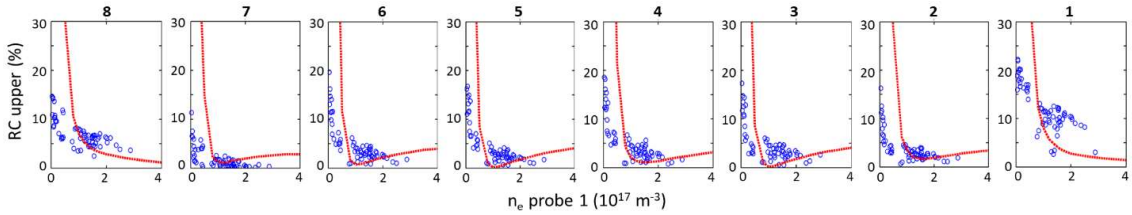

FIG. 5. RC in each module on the upper part of the LH1 launcher versus density measured by a Langmuir probe on the upper part of LH1. The curves show the ALOHA-modelling using two density gradients (λ_1 = 1 mm; λ_2 = 15 mm).

In contrast, the RC on the individual modules on the PAM/LH2 launcher behave differently depending on their toroidal location (Fig. 6). An increase in RC with increasing edge density is seen on the lateral modules, while the opposite behaviour is observed on the central modules. A comparison with ALOHA is not shown in Fig. 6, because there is no single ALOHA-run that gives agreement with the experimental values in all modules simultaneously. The ALOHA-calculations however suggest that the edge density in front of the lateral modules is higher than that in front of the central modules, which is consistent with the fact that the LH2 launcher has not been reshaped.

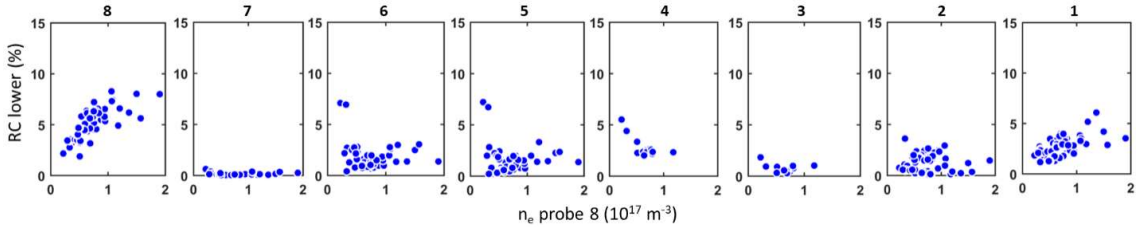

FIG. 6. RC in each module on the lower part of the LH2 launcher versus density measured by a Langmuir probe on the lower part of LH2. The RC on the lateral modules (1 and 8) show the opposite behaviour to that on the central modules.

4. HEAT LOAD ON THE LAUNCHERS DURING LONG PULSE OPERATION

A series of long pulse discharges (~ 50 s) have been carried out in WEST to study the ammonia formation during Nitrogen seeding [9]. These pulses used LHCD power at a level of 3 MW to provide the necessary current drive to assure the pulse length required. Figure 7 shows the main plasma parameters for a typical long pulse discharge, with plasma current I_P = 400 kA, toroidal field B_T = 3.7 T, P_{LH} = 3.0 MW, central line integrated electron density n_{li} = 3.3×10^{19} m^{-2} in L-mode and USN configuration. The LH power was split between 1.6 MW from the LH1 launcher and 1.4 MW from the LH2 launcher.

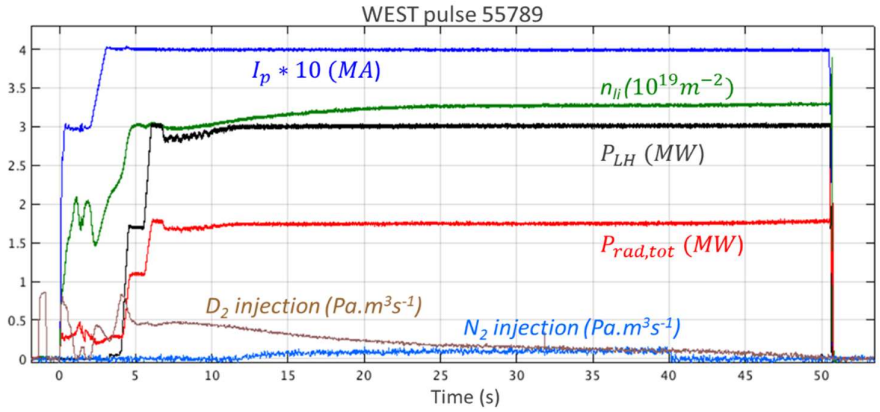

FIG. 7. Main plasma parameters for pulse #55789: Plasma current (I_P), central line integrated density (n_{li}), lower hybrid power (P_{LH}), total radiated power ($P_{rad,tot}$), D_2 and N_2 injection rates.

The infrared (IR) imaging system in WEST [10] provides the measurement of the apparent front face temperature (i.e. assuming emissivity equal to 1.0) during the pulses. During these long pulses, an inhomogeneous temperature increase was observed on the LH2 launcher. The walls of the passive waveguide on the edges of the LH2 launcher increased much faster in temperature than the centre of the launcher. This is visualised in Fig. 8. The overheating on the edge modules comes from the fact that the LH2 launcher has not yet been reshaped toroidally to fit the toroidal curvature of the plasmas in WEST. Electrons accelerated in front of the grill mouth by the LH electric field follow the magnetic field lines and can hit the edge of the launcher itself if the launcher is not well adapted to the toroidal curvature of the field lines. In contrast, such overheating has not been observed on the LH1 launcher during long pulses in WEST [11], which again proves that the toroidal reshaping of LH1 has been successful. The IR measurements of LH1 for the series of discharges in Fig. 7 are not shown here, but earlier data from 30 s long pulses reveal that the temperature increase on LH1 is weak and homogeneous on the central and edge modules

[11]. It has now been decided to reshape also the LH2 launcher to avoid overheating on the launcher mouth when extending the WEST pulse duration even further. The goal for the 2021 experimental campaign is to reach 120 s long pulses.

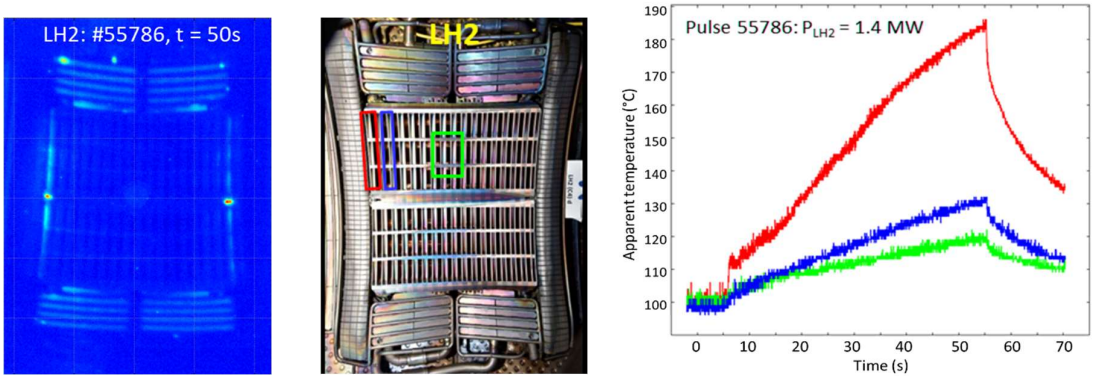

FIG. 8. Infrared (IR) image of the LH2 launcher for the 55 s long discharge #55786 (left). Photo of the LH2 launchers with three zones indicated (middle). Apparent IR temperature for the three zones for pulse #55786 (right). The power on the LH2 launcher was 1.4 MW.

5. EFFECT OF PLASMA CONFIGURATION ON THE LH COUPLING

Several magnetic equilibria have been explored in the last WEST campaigns in 2020-2021 aiming at high power and high confinement discharges. The four main equilibria are illustrated in Fig. 9. Both USN and LSN configuration were used, having different X-point heights and different position of the last closed flux surface at the mid-plane (R_{ext}). The LH launchers were positioned approximately 4 cm away from R_{ext}, i.e. $R_{LH} \sim 2.95$ m for the configurations with $R_{ext} = 2.91$ m and $R_{LH} \sim 3.01$ m for the configurations with $R_{ext} = 2.97$ m. Fig. 10 shows the average reflection coefficient (RC) on the upper and lower rows of LH1 versus the radial outer gap measured at Z = +0.25 m and Z = -0.25m, i.e. in front of the upper and lower rows of LH1. All data points in Fig. 10 correspond to time slices with coupled lower hybrid power (P_{LH}) > 0.5 MW, plasma current between 480 kA and 500 kA and central line integrated density between 2.5 and 6.2 $\times 10^{19}$ m^{-2}. In particular for the upper rows, the reflection coefficient is very sensitive to the plasma configuration and a large variation in reflection coefficient is observed even for the same plasma-launcher gap.

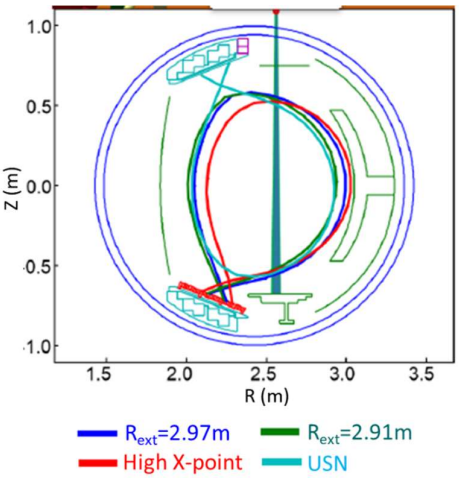

FIG. 9. The four different plasma configurations explored in the latest WEST experiments.

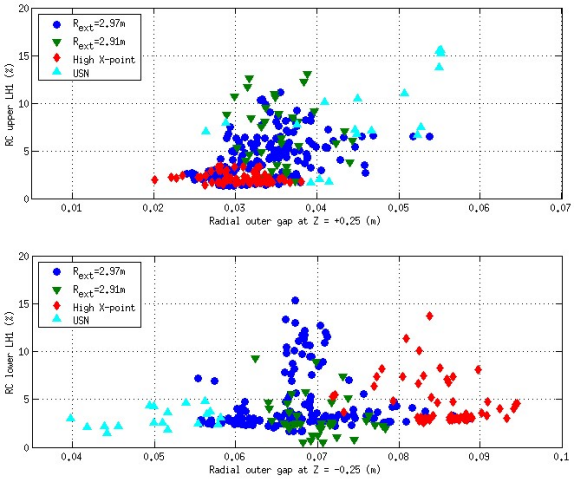

FIG. 10. RC on the upper and lower parts of LH1 versus the radial outer gap deduced from the NICE equilibrium reconstruction for the upper and lower rows of LH1.

The dependence on plasma density is shown in Fig. 11 where the RC are plotted versus the central line integrated density. One finds again that RC on the upper part of LH1 differs significantly in the different plasma configuration even for the same density. This means that the density in front of the upper part of the LH grill is dependent on the details of the plasma equilibria. On the lower part, however, the variation in RC is much smaller and one finds a good correlation between RC and the central density, which means that the density in front of the lower part of the grill follows well the central plasma density. An even better correlation is found when plotting RC for the lower part of LH1 versus the density at the outer divertor target, measured by a Langmuir probe in the lower divertor, for the three equilibria in LSN configuration (Fig. 12). Comparing Fig. 12 and Fig. 10, one can conclude that the coupling for the lower part of LH1 is more dependent on the density at the outer divertor target than on the plasma-launcher gap at -0.25 m. The same dependence is not found for the upper rows of LH1. For the upper rows, the coupling is found to be very sensitive to plasma configuration and the coupling gets better for larger R_{ext}, even though the plasma-launcher gap is the same according to the equilibrium reconstruction. Higher RC is systematically seen on the upper rows of LH1 in the configurations with R_{ext} = 2.91 m. A possible explanation could be that the toroidal shaping of the LH1 launcher is better optimised for a working position of R_{LH} ~ 3.01 m rather than further inwards.

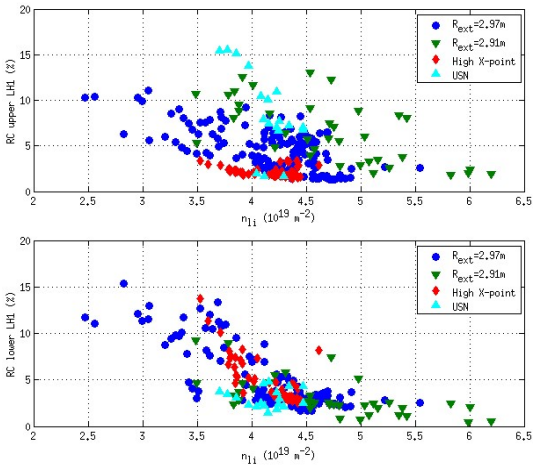

FIG. 11. RC on the upper and lower rows of LH1 versus central line integrated density.

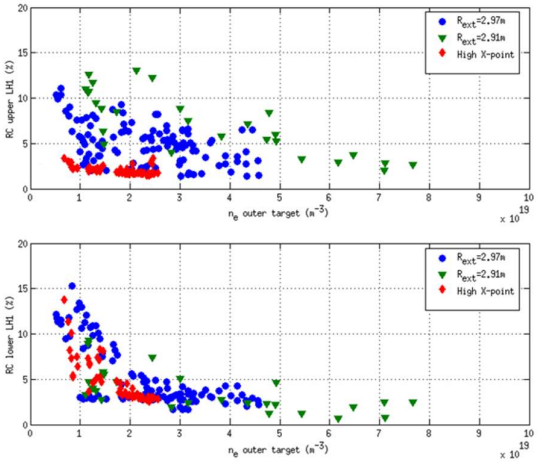

FIG. 12. RC on the upper and lower rows of LH1 versus the density measured at the outer divertor target for the three configurations in LSN.

6. SUMMARY AND CONCLUSIONS

The first phase of WEST is now completed and the experiments have shown that the LHCD system is capable of providing RF power in a wide range of plasma configurations. Up to 5.3 MW has been coupled in L-mode plasmas and 55 s long pulses have been sustained with LHCD power of 3 MW. The toroidal reshaping of the LH1 launcher that was made before its installation in WEST has proven successful, i.e. good coupling can be obtained on all modules simultaneously if the density in front of the launcher mouth is sufficiently high. The experiments have also demonstrated that the reshaping of the LH2 launcher is necessary to avoid overheating on the launcher front when aiming for longer pulses (120 s and more).

ACKNOWLEDGEMENTS

This work has been carried out within the framework of the EUROfusion Consortium and the French Research Federation for Fusion Studies and has received funding from the Euratom research and training programme 2014-2018 and 2019-2020 under grant agreement No 633053. The views and opinions expressed herein do not necessarily reflect those of the European Commission.

REFERENCES

[1] BUCALOSSI, J., et al., "Operating a full tungsten actively cooled tokamak: overview of WEST first phase of operation", this conference.
[2] HILLAIRET, J., et al., "WEST actively cooled load resilient ion cyclotron resonance heating results", this conference.
[3] DELPECH, L., et al., Fusion Eng. Des. **96-97** (2015) 452-457.
[4] EKEDAHL, A., Nucl. Fusion **50** (2010) 112002.
[5] GONICHE, M., et al., "Developing high performance RF heating scenarios on the WEST tokamak", this conference.
[6] FAUGERAS, B., et al., Fusion Sci. Technol. **69** (2016) 495-504.
[7] NOUAILLETAS, R., et al., Fusion Eng. Des. **146** (2019) 999-1002.
[8] HILLAIRET, J., et al., Nucl. Fusion **50** (2010) 125010.
[9] LOARER, T., et al., Nucl. Fusion **60** (2020) 126046.
[10] COURTOIS, X., et al., Fusion Eng. Des. **146** (2019) 2015-2020.
[11] DELPECH, L., et al., AIP Conf. Proc. **2254** (2020) 080004.